Journal of the Brazilian Society of Mechanical Sciences and Engineering (2019) 41:374
https://doi.org/10.1007/s40430-019-1869-6

TECHNICAL PAPER

Simulation of fatigue cracks growth processes of two parallel cracks in thin plate pulled by the constant amplitude cyclic loading

X. Q. Zhang[1] · J. Wang[1] · W. Wei[1,2] · X. T. Ji[1] · B. Chen[1] · G. W. Fang[1]

Received: 3 December 2018 / Accepted: 14 August 2019 / Published online: 24 August 2019

Abstract
In the paper, the propagation processes of two parallel cracks in 2-mm-thick plate pulled by the cyclic loading were investigated by numerical simulation and experiment. The codes Abaqus and Franc3D were implemented jointly to predict the crack growth path, the stress distribution around the cracks tip and the fatigue life. The corresponding fatigue experiment was carried out on a servo-hydraulic fatigue testing machine. The investigation indicates that the predicted crack paths agree well with the experimental results at the crack propagation early stage, and the predicted crack growth rate is consistent with the findings in experiment, which validate the prediction of the mixed mode crack propagation processes.

Keywords Fatigue crack growth · Thin plate · Finite element method · Stress intensity factor · Crack path

1 Introduction

Fatigue cracks generally initiate at the stress concentration regions of structure component subjected to cyclic loading, such as notches, holes, fillets and welds. The micro-cracks progressively grow under the action of cyclic loading and finally lead to structure failure abruptly, which may result in heavy casualties and enormous economic losses. Therefore, it is a necessity to grasp the mechanism of fatigue fracture to avoid the accident occurrence.

So far, a series of attempts have been made to gain insight into the crack growth behaviors. In order to evaluate crack extension direction, some criteria are proposed, such as the maximum tangential stress (MTS) criterion [1, 2], the maximum energy release rate (MERR) criterion [3], the minimum strain energy density (MSED) criterion [4], the maximum strain (MS) criterion [5], the maximum principle stress (MPS) criterion [6, 7], the maximum shear stress (MSS) criterion [8] and the averaged strain energy density (ASED) [9]. Furthermore, to assess the fatigue crack propagation rate, some rules have been put forward, such as Paris equation [10] and NASGRO model [11]. And to judge whether the fatigue crack enters the stage of rapid instability expansion or not, the stress intensity factor (SIF) is raised [12], which has been widely applied in practice [11, 13, 14].

Stress concentration generally locates at manufacturing defect regions or a location where the geometrical shape of the object changes drastically, such as the lap joints and rivet holes [15–17]. The numbers of investigations on cracks originating from those regions have been constantly conducted. He et al. [18] have investigated the growth of asymmetric cracks at the edge of the hole to evaluate the fatigue life under idealized mode I condition. Boljanovic et al. [19] have also utilized an initial crack at the edge of hole with 20-mm diameter in aluminum alloy plate to analyze the crack growth propagation under the mixed mode (I/II) loading. Zhang et al. [6] have examined the influence of the size and location of the hole on the crack growth behavior using experimental and numerical methods, and the results indicate that the fatigue crack propagates toward the hole. Blažić et al. [20] have researched the growth trajectory of crack between two separate holes under an initial mixed mode I/II condition. Their researches show that two cracks are parallel to propagate in the opposite direction under the external force, and that the influence of the small hole on

Technical Editor: André Cavalieri.

✉ X. Q. Zhang
zhang20020313@163.com

J. Wang
201225040412@chd.edu.cn

[1] School of Mechanical Engineering, Anhui University of Technology, Ma'anshan 243002, China

[2] Faculty of Mechanical Engineering and Automation, Zhejiang Sci-Tech University, Hangzhou 310018, China

the crack path becomes more obvious when the crack length increases. The investigations give an insight on the crack growth behaviors affected by a single hole or two ones. However, there are relatively few studies on propagation process of two central symmetric cracks emanating from two adjacent holes, respectively, under the mixed mode condition and some characteristics of crack propagation are still unknown.

This paper attempts to investigate the propagation process of two mixed mode cracks, which originate from two adjacent holes in a 7075-T6 aluminum alloy plate pulled by constant amplitude cyclic loading. It focuses on the fatigue crack growth (FCG) path, the stress distribution around the cracks tip as well as the SIF values at different crack extension steps with numerical simulation. The experiments for verification are also carried out. The results indicate that the predicted crack propagation paths as well as the predicted FCG rate are consistent well with the experimental results. The investigation provides certain reference for predicting the crack propagation in cracked components in engineering.

2 Related theoretical bases

2.1 Crack growth angle

During FCG, the kink angle θ determines the orientation of new crack front. As mentioned above, several criteria, such as MTS, MERR and MSED, have been used to compute the direction of the crack growth, and the MTS criterion is more popularized. Herein, it is also employed. According to the isotropic linear elastic fracture theory [21], the kink angle of the crack growth under the mixed mode (I/II) condition can be expressed as:

$$\theta_0 = 2\arctan\frac{1}{4}\left[\frac{K_{\mathrm{I}}}{K_{\mathrm{II}}} \pm \sqrt{\left(\frac{K_{\mathrm{I}}}{K_{\mathrm{II}}}\right)^2 + 8}\right] \tag{1}$$

2.2 FCG rate model

In general, the FCG process comprises three stages, namely the crack initiation, stable propagation and unstable rapid growth stage, and the FCG rate curve can also be divided into three parts: the near threshold part, the linear part and the near-critical part [22]. The widely used Paris equation is only valid to compute the FCG rate for the linear part and is ineffective for the others. While the NASGRO model is applicable for the whole process of fatigue crack growth, which is [7, 11]:

$$\frac{\mathrm{d}a}{\mathrm{d}N} = C\left[\Delta K(1-f)/(1-R)\right]^n \frac{\left(1-\Delta K_{\mathrm{th}}/\Delta K\right)^p}{\left(1-K_{\max}/K_{\mathrm{c}}\right)^q} \tag{2}$$

where a represents crack length and N stands for the number of cycles. C and n are used to describe the material characteristic, which resemble the parameters in Paris equation [10]; ΔK is SIF range; f is a function illustrating the crack front closure [23]; R is the applied stress ratio; p and q are exponents to describe the curvature near the threshold part and critical part, respectively; and ΔK_{th} is the range of the threshold SIF, below which crack will not propagate and can be described in Ref. [7]. $K_{\max}$ and K_{c} are the maximum SIF and critical SIF, respectively. The values of these parameters in the model often can be selected in material database of NASGRO v3 package embedded in the code Franc3D when typical materials are used. Presently, the material 7075-T6 aluminum alloy is researched and the parameters can be obtained directly from the material database [24].

3 Numerical simulation

3.1 Process of FCG

To investigate the propagation process of the mixed mode cracks, the finite element codes Abaqus and Franc3D were employed jointly to predict the FCG path and compute the SIF, respectively. The code Abaqus embodies three main modules, Abaqus/Explicit, Abaqus/Standard and Abaqus/CFD. Abaqus/Explicit is applicable to deal with the transient dynamic problems like high speed shocking. And Abaqus/Standard is a static analysis module and can handle the numbers of linear and nonlinear issues. As for Abaqus/CFD, it is generally applied in fluid mechanics. In this paper, Abaqus/Standard is utilized for modeling and stress analysis. The code Franc3D is a specialized software for analyzing crack growth behaviors.

During simulation, the Abaqus/Standard is used first to create the 3D finite element model, to analyze the stress field and to determine the location of the maximum stress, where the micro-crack is prone to nucleate. Subsequently, according to the Abaqus/Standard analysis results, the Franc3D is utilized to insert an initial crack into the created model at the maximum stress location and to remesh the model. Then, the Abaqus is employed again to execute stress analysis. After that, the SIFs at the crack front can be determined in Franc3D based on the stress analysis results obtained from Abaqus. When it does not meet $K_{\mathrm{equiv}} \geq K_{\mathrm{C}}$ or $\Delta K < \Delta K_{\mathrm{th}}$, the crack will propagate continuously in Franc3D and the above analysis steps will not finish until the condition is satisfied. Figure 1 depicts a brief flowchart of the utilization of the Abaqus and Franc3D during simulation, and the detailed analysis process of current case is as follows.

The finite element model of plate with two small holes and parallel cracks was first established using the code Abaqus, whose dimension was $91 \times 60 \times 2$ mm

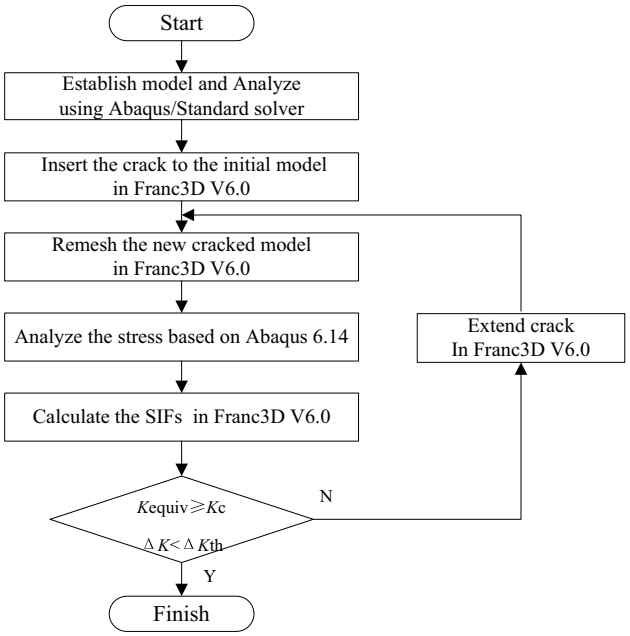

Fig. 1 Flowchart of crack propagation simulation

(length × width × thickness). The diameter of the holes was 4 mm, and the cracks were 5 mm long, as depicted in Fig. 2. The elastic modulus and Poisson's ratio were 71.7 GPa and 0.3, respectively. Element-type C3D8R, an eight-node hexahedral linear reduced integration unit, was used to mesh the developed geometrical model. The top edge of the model was fixed, and movement and rotation of nodes on the clamped edge are constrained. The bottom end was pulled by a cyclic load with loading ratio of 0 and maximum value of 8 kN which was distributed evenly over a length of 60 mm, as shown in Fig. 2. After the stress calculation with Abaqus, the maximum stress and its location could be determined. Then, the *.inp* file could be obtained and exported from Abaqus.

Subsequently, the *.inp* file mentioned above was read in Franc3D, and the penetrating crack with its length 0.4 mm was inserted manually into two parallel crack tips, where the maximum stress was located. Then, the model with inserted micro-cracks was remeshed in Franc3D, as revealed in Fig. 3. Figure 4 demonstrates the meshes around the crack tip, where there are two kinds of elements: 15-node singular wedge element at the inner ring and 20-node hexahedral element at the outer ring. As a result of such meshing, the stress at the crack tip could avoid tending to infinity when the external loading was imposed [25]. The remeshed model and its corresponding information were stored into a database *fdb*. file in Franc3D.

Afterward, Franc3D would attempt to execute static crack analysis of the remeshed model based on the Abaqus Batch/Executable information, and the results obtained from the previous step were utilized to compute the SIFs at the crack front. The above-presented procedures were repeated multiple times, and the fatigue crack path and the SIFs along the crack front at different steps could be obtained.

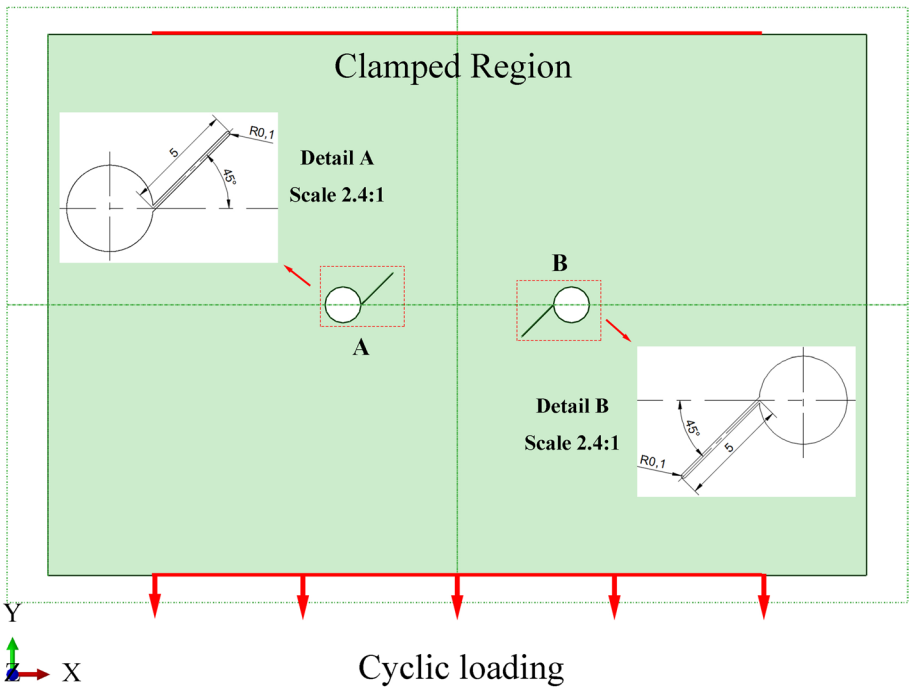

Fig. 2 Initial finite element model developed in Abaqus

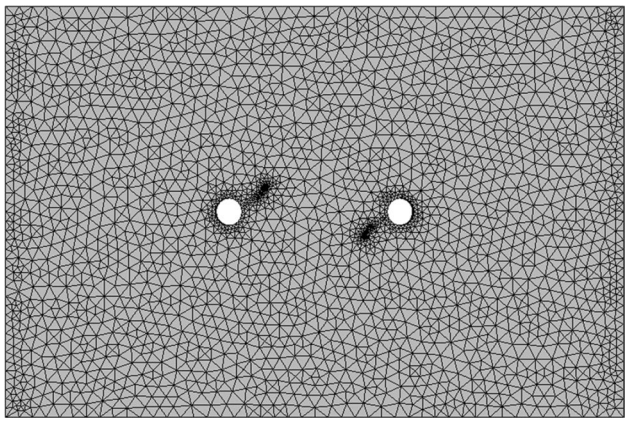

Fig. 3 Remeshed model after inserting two initial cracks into the previous model

3.2 Numerical simulation process of FCG

According to above-mentioned procedure, the propagation process of two parallel cracks under the mixed mode condition has been obtained. Figure 5 displays the FCG paths as well as stress distribution around the cracks tip at different crack extension steps. In order to see clearly the crack growth path, the displacement in the model has been magnified by 15 times. From Fig. 5, it can be seen that, at the 13th extension step (Fig. 5b), the surface crack grows 8.9 mm, and the predicted number of cycles is 65,037 cycles. At the 17th step (Fig. 5c), the crack length reaches 10.4 mm, and the corresponding number amounts to 73,015 cycles. At the 30th step (Fig. 5e), the crack length is increased to 13.5 mm accompanied with 84,576 cycles. Subsequently, the crack grows 14.6 mm along the direction perpendicular to the external loading when it is imposed by cyclic loading with the number of 87,982 cycles, as demonstrated in Fig. 5e–h. When the crack grows 15.6 mm with 91,248 cycles in Fig. 5i, it approaches to the opposite hole, and its growth direction changes obviously and turns toward the opposite hole, as reported in previous references [7, 26].

Fig. 5 Crack growth path captured from 1st to 70th steps (15 times magnification of the model's displacement has been conducted) **a** 1st, **b** 13th, **c** 17th, **d** 26th, **e** 30th, **f** 40th, **g** 46th, **h** 47th, **i** 52th and **j** 70th

Figure 5 also illustrates the stress distribution around the cracks tip at different crack extension steps, which can explain the causes of the above-described crack paths. At the 1st crack extension step, the stress field is independent and only located around the crack tip. With the increase in the cracks length, the area of stress field around the cracks tip enlarges continuously. At the 13th step, two previous independent stress fields connect together (Fig. 5b). At the 30th step (Fig. 5e), the contour of the merged stress field is approximately parallel to the loading direction. After this step, the crack begins to grow toward the opposite hole. At the 46th step (Fig. 5g), the merged stress field starts to separate, and to the 52nd step (Fig. 5i), it is divided into two separate ones thoroughly. Subsequently, the area of two stress fields progressively becomes small around the crack tips when the crack approaches to the opposite hole. In short, the stress field around the cracks tip has experienced three stages: separating–merging–separating. Moreover, it can also be seen from Fig. 5 that the stress field at the hole edge opposite to the cracked edge alters constantly. The intensity and domain of the stress field gradually increase due to the lessening cross section between two holes as well as the stress concentration. However, there is no crack propagation, because there is no initial crack insertion at this location in simulation.

3.3 Calculation of SIFs

After the stress calculation with the Abaqus, the SIF values can be figured out by M-integral [27] in code Franc3D. Figure 6 shows the SIF values taken from the median location of the crack front at different crack extension steps. The values at the 1st step are shown in Fig. 6a, from which K_{I} and K_{II} range from 200 to 250 MPa mm$^{1/2}$ and 170 to 225 MPa mm$^{1/2}$, respectively, while K_{III} varies from -20

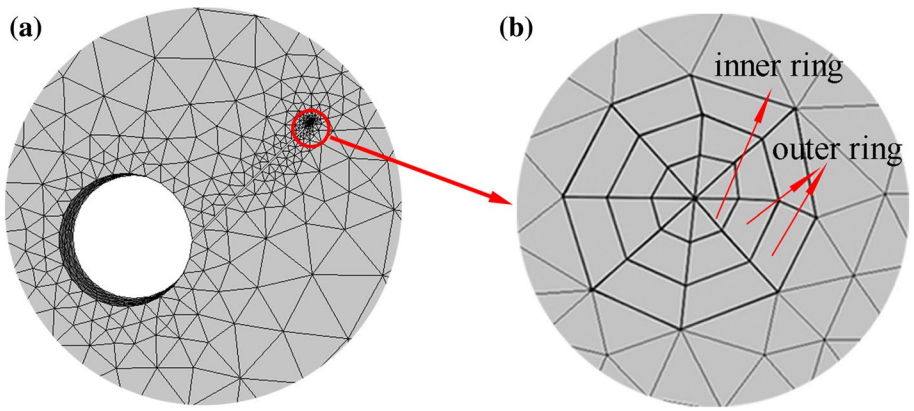

Fig. 4 Meshed small hole and initial crack **a** overall view of the meshed hole and inserted crack, **b** meshes of the inserted crack tip

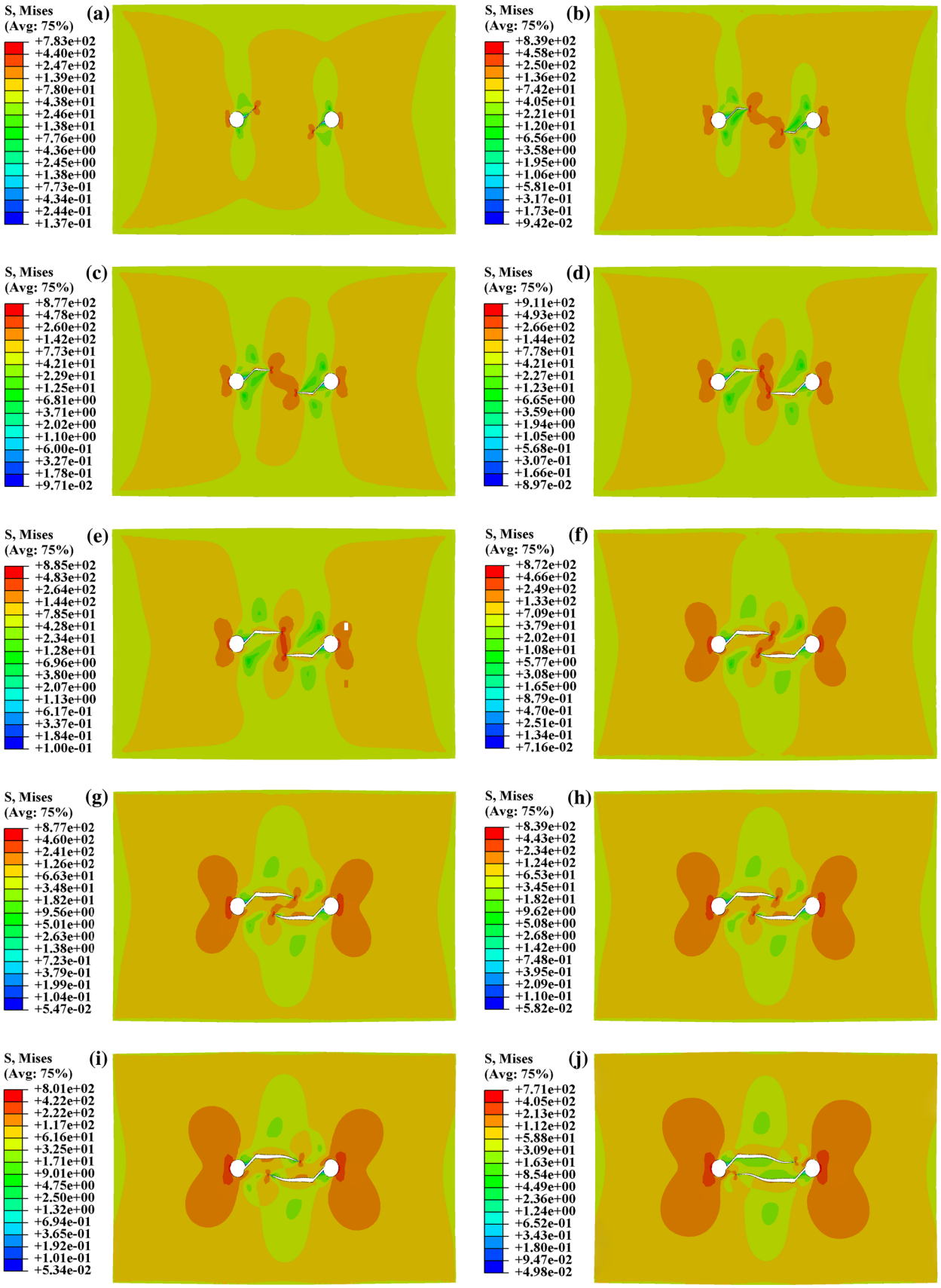
S, Mises
(Avg: 75%)
(a)
+7.83e+02
+4.40e+02
+2.47e+02
+1.39e+02
+7.80e+01
+4.38e+01
+2.46e+01
+1.38e+01
+7.76e+00
+4.36e+00
+2.45e+00
+1.38e+00
+7.73e-01
+4.34e-01
+2.44e-01
+1.37e-01
S, Mises
(Avg: 75%)
(b)
+8.39e+02
+4.58e+02
+2.50e+02
+1.36e+02
+7.42e+01
+4.05e+01
+2.21e+01
+1.20e+01
+6.56e+00
+3.58e+00
+1.95e+00
+1.06e+00
+5.81e-01
+3.17e-01
+1.73e-01
+9.42e-02
S, Mises
(Avg: 75%)
(c)
+8.77e+02
+4.78e+02
+2.60e+02
+1.42e+02
+7.73e+01
+4.21e+01
+2.29e+01
+1.25e+01
+6.81e+00
+3.71e+00
+2.02e+00
+1.10e+00
+6.00e-01
+3.27e-01
+1.78e-01
+9.71e-02
S, Mises
(Avg: 75%)
(d)
+9.11e+02
+4.93e+02
+2.66e+02
+1.44e+02
+7.78e+01
+4.21e+01
+2.27e+01
+1.23e+01
+6.65e+00
+3.59e+00
+1.94e+00
+1.05e+00
+5.68e-01
+3.07e-01
+1.66e-01
+8.97e-02
S, Mises
(Avg: 75%)
(e)
+8.85e+02
+4.83e+02
+2.64e+02
+1.44e+02
+7.85e+01
+4.28e+01
+2.34e+01
+1.28e+01
+6.96e+00
+3.80e+00
+2.07e+00
+1.13e+00
+6.17e-01
+3.37e-01
+1.84e-01
+1.00e-01
S, Mises
(Avg: 75%)
(f)
+8.72e+02
+4.66e+02
+2.49e+02
+1.33e+02
+7.09e+01
+3.79e+01
+2.02e+01
+1.08e+01
+5.77e+00
+3.08e+00
+1.65e+00
+8.79e-01
+4.70e-01
+2.51e-01
+1.34e-01
+7.16e-02
S, Mises
(Avg: 75%)
(g)
+8.77e+02
+4.60e+02
+2.41e+02
+1.26e+02
+6.63e+01
+3.48e+01
+1.82e+01
+9.56e+00
+5.01e+00
+2.63e+00
+1.38e+00
+7.23e-01
+3.79e-01
+1.99e-01
+1.04e-01
+5.47e-02
S, Mises
(Avg: 75%)
(h)
+8.39e+02
+4.43e+02
+2.34e+02
+1.24e+02
+6.53e+01
+3.45e+01
+1.82e+01
+9.62e+00
+5.08e+00
+2.68e+00
+1.42e+00
+7.48e-01
+3.95e-01
+2.09e-01
+1.10e-01
+5.82e-02
S, Mises
(Avg: 75%)
(i)
+8.01e+02
+4.22e+02
+2.22e+02
+1.17e+02
+6.16e+01
+3.25e+01
+1.71e+01
+9.01e+00
+4.75e+00
+2.50e+00
+1.32e+00
+6.94e-01
+3.65e-01
+1.92e-01
+1.01e-01
+5.34e-02
S, Mises
(Avg: 75%)
(j)
+7.71e+02
+4.05e+02
+2.13e+02
+1.12e+02
+5.88e+01
+3.09e+01
+1.63e+01
+8.54e+00
+4.49e+00
+2.36e+00
+1.24e+00
+6.52e-01
+3.43e-01
+1.80e-01
+9.47e-02
+4.98e-02

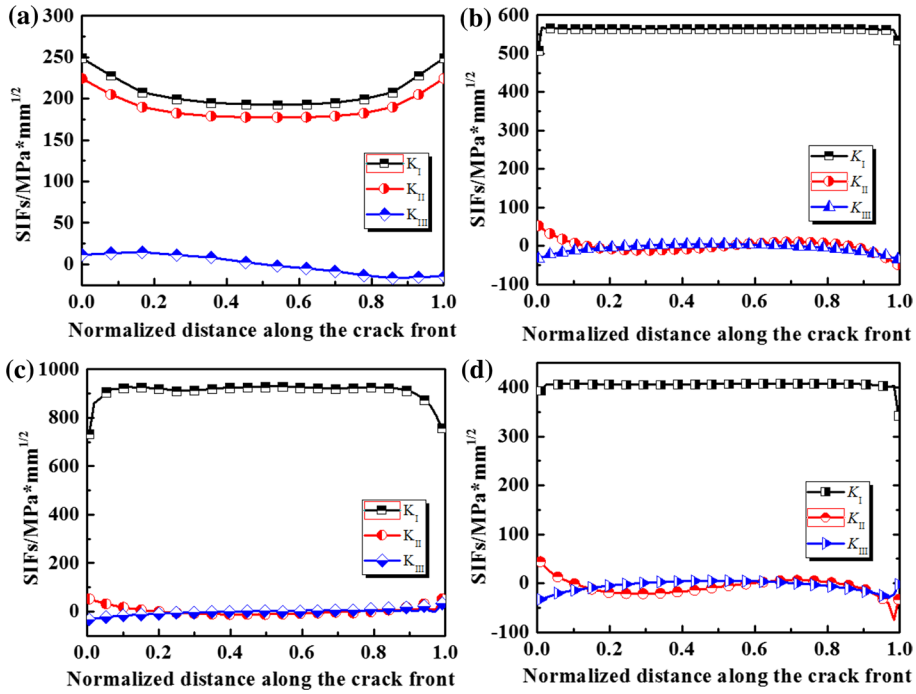

Fig. 6 SIFs of the crack front at different crack extension steps **a**, **b**, **c** and **d** show the SIFs at the 1st, 15th, 30th and 50th step, respectively

to 20 MPa mm$^{1/2}$. The results exhibit that the values of K_I and K_{II} are greater than that of K_{III}, which manifests that the initial crack belongs to I/II mixed mode crack.

Compared with the SIFs at different steps, K_I is first increased to 929.80 MPa mm$^{1/2}$ at 30th step and then decreased to 408.39 MPa mm$^{1/2}$ at 50th step. During these steps, K_I is greater than K_{II} and K_{III}. Therefore, the mode I is predominant in the following steps.

4 Fatigue tensile experiments

4.1 Experimental conditions

According to developed model shown in Fig. 2, the dimension of samples was 91 × 60 × 2 mm (length × width × thickness). They were cut directly from a commercial product 7075-T6 aluminum alloy plate by wire electrical discharge machining (WEDM) method. Two small holes with Φ4 mm diameter were drilled, respectively, at location of 12.7 mm away from the vertical centerline of the plate. Two parallel cracks with 5-mm length were also fabricated by WEDM method, whose positions were 45° geometric angle with respect to the horizon direction, and the load was imposed along the vertical direction in experiment, as displayed in Fig. 7.

The fatigue tensile experiments were carried out on a 100 kN/500 Nm servo-hydraulic fatigue testing machine. During experiments, the specimens were clamped by the upper and lower chucks of the setup, respectively, as

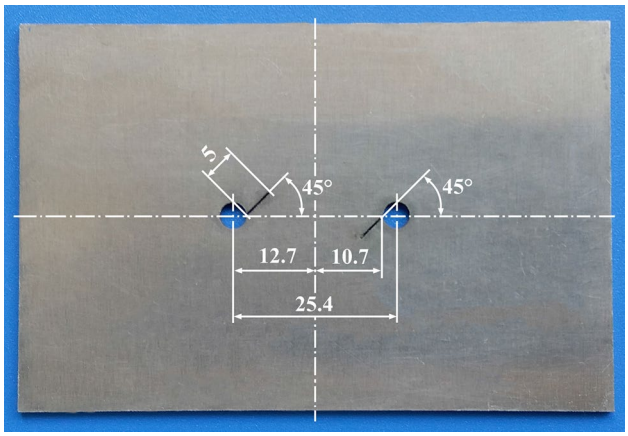

Fig. 7 Geometry of the samples employed in the experiments

displayed in Fig. 8. The location of upper chuck was fixed, and the lower one was driven by hydraulic cylinder. The tests were conducted at room temperature of 25 °C, and the applied parameters in current case are tabulated in Table 1 in detail.

4.2 Experimental results

Figure 9 briefly reveals the fatigue growth processes of two mixed mode cracks under constant amplitude loading, which are recorded by an industrial camera at a certain time interval. The number of cycles is also counted by the computer. As shown in Fig. 9, the length of two cracks increases

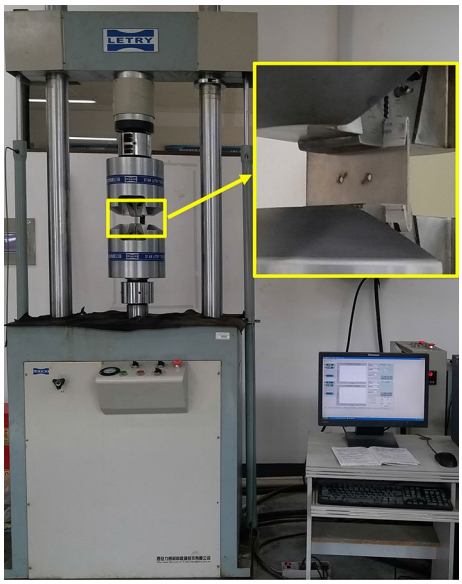

Fig. 8 Experimental condition as well as the sample

Table 1 Experimental parameters

Parameters	Numerical value
Load amplitude F	8 (kN)
Stress ratio R	0
Load type	Sinusoidal loading
Frequency	15 (Hz)
Testing machine model	PLN-100/500

progressively with the enhancement of the number of cycles, and the length of two fatigue cracks is roughly equal and the trajectories are similar. Under the function of cyclic loading, the cracks start propagating due to stress concentration at the cracks tip. When the number of cycles is about 57,282 cycles, the lengths of two cracks grow approximately 8.8 and 8.6 mm, respectively. When it is up to nearly 71,150 cycles, two lengths are increased to 10.6 and 10.5 mm, respectively. To 80,696 cycles, the corresponding values are about 12.7 and 12.4 mm. And then to about 93,583 cycles, they reach to 15.8 and 15.4 mm, respectively, as displayed in Fig. 9e. Meanwhile, new micro-cracks can be observed at the hole edge opposite to the cracked side. When it adds up to 130,372 cycles, the cracks grow 18.5 and 17.4 mm, respectively, and approach to the edge of opposite hole. At the same time, the newborn cracks also grow further, as shown in Fig. 9f.

4.3 Comparison between the experimental data and simulation results

Figure 10 depicts the relationship between the crack length a and the corresponding number of cycles N according to the test data. Here, the crack length a refers to the average values of two above-mentioned cracks. In order to compare directly, the predicted results are also plotted. In Fig. 10, when the length of crack is about 8.8 mm, the number of cycles is about 57,282 cycles in experiments, while the predicted value is 64,562 cycles in simulation, which deviates roughly 12.7% from the experimental value. When the crack length reaches about 10.6 mm, the corresponding experimental and numerical results are 71,152 and 73,815 cycles, respectively, and the deviation between them is about 3.7%, which indicates that the experimental curve is consistent with the predicted one. It also can be seen from Fig. 10 that both the numerical and experimental curves, a versus N, become steeper and steeper at the early stage of crack

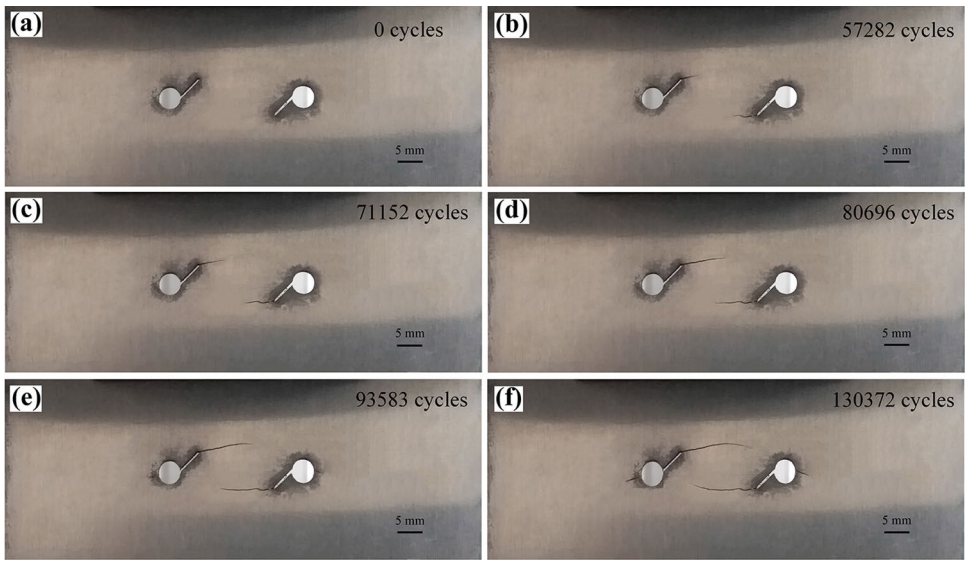

Fig. 9 Propagation processes of two pre-cracks under experimental condition

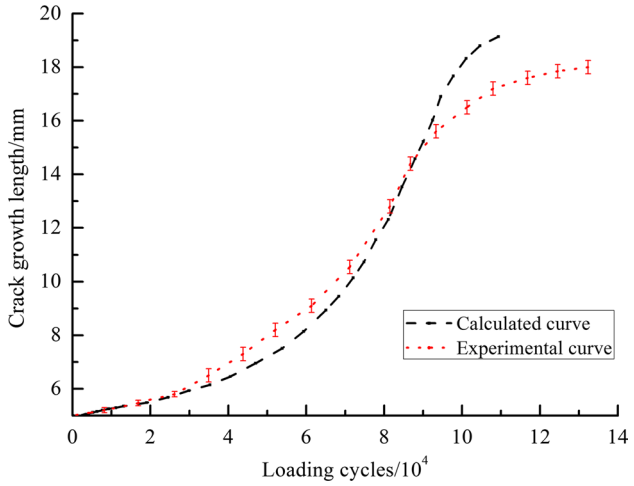

Fig. 10 Crack length versus load cycles

propagation when the number of cycles is increased, which indicates that the cracks grow faster and faster. However, at the later stage of crack propagation, the experimental curve progressively tends to flat, which indicates that the crack growth rate becomes slow. The experimental data obviously deviate from the predicted ones, which are attributed to two new cracks generated at the hole edge side opposite to the initial cracked one. The newer crack propagation consumes much energy and correspondingly reduces pre-crack growth driving force, so the pre-crack growth rate slows down when the newer cracks occur at the higher number of cycles. In order to decrease stress concentration to inhibit the crack initiation at the hole edge, some surface processing technologies are employed to induce compressive residual stress such as shot peening and laser shot peening [28–31].

Figure 11 displays the predicted FCG paths and experimental ones. From Fig. 11, it can be seen that they have a similar tendency and the predicted ones deviate slightly from the test results, which verify the correctness of the numerical simulation. In addition, the propagation path of prefabricated

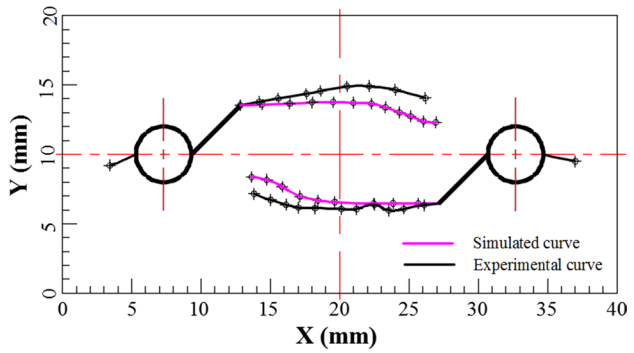

Fig. 11 Crack propagation paths obtained by numerical simulation and experiments

crack stemming from the left side is central symmetric to the one from the right side and it has also been reported in Ref. [15], which also validates the established model further.

5 Conclusions

In the paper, the fatigue growth process of the mixed mode cracks has been investigated by FEM and fatigue tensile tests. The predicted results are consistent with the findings in experiments. Several conclusions can be drawn as followings:

1. Under the constant amplitude cyclic loading, the stress fields around the cracks tip vary continuously. The dominant mode of cracks in thin plate turns into mode I from the initial mixed mode I/II.
2. When acted by external fatigue loading, two centrosymmetrical cracks in thin plate grow faster and faster. The stress fields around the crack tips are centrosymmetrical, and their growth paths are also centrosymmetrical.
3. The intensity of stress field at the hole edge side opposite to the cracked side becomes stronger with the length enhancement of two prefabricated cracks, and its area also becomes larger.
4. The code Franc3D together with Abaqus can effectively predict the propagation processes of two parallel cracks in thin plate.

Acknowledgements The authors are grateful for the support provided by the National Natural Science Foundation of China (Nos. 51675002, 51175002), National Natural Science Foundation of Anhui province (No. 1708085ME110), Natural Science Foundation of Colleges and Universities in Anhui province (No. KJ2016A813), Key Research and Development Projects in Anhui (201904a05020065), Open Foundation of Zhejiang Provincial Top Key Academic Discipline of Mechanical Engineering (ZSTUME02A05) and the Natural Science Research Projects of Universities in Anhui Province (No. KJ2019A0084).

Compliance with ethical standards

Conflict of interest The authors declare that they have no conflict of interest.

References

1. Erdogan F, Sih GC (1997) On the crack extension in plates under plane loading and transverse shear. J Basic Eng 12(4):527
2. Mirsayar MM, Park P (2016) Modified maximum tangential stress criterion for fracture behavior of zirconia/veneer interfaces. J Mech Behav Biomed Mater 59:236–240
3. Palaniswamy K, Knauss WG (1972) Propagation of a crack under general, in-plane tension. Int J Fract Mech 8(1):114–117
4. Sih GC (1974) Strain-energy-density factor applied to mixed mode crack problems. Int J Fract 10(3):305–321

5. Chang KJ (1981) On the maximum strain criterion—a new approach to the angled crack problem. Eng Fract Mech 14(1):107–124
6. Zhang XQ, Zhang X, Li L (2016) Investigation of the influence of small hole on the fatigue crack growth path. J Fail Anal Prev 16(3):391–399
7. Meng Q, Wang Z (2014) Extended finite element method for power-law creep crack growth. Eng Fract Mech 127:148–160
8. Yu X, Li L, Proust G (2017) Fatigue crack growth of aluminum alloy 7075-T651 under proportional and non-proportional mixed mode I and II loads. Eng Fract Mech 174:155–167
9. Moghaddam MR, Ayatollahi MR, Berto F (2017) Mixed mode fracture analysis using generalized averaged strain energy density criterion for linear elastic materials. Int J Solids Struct 120:1339–1351
10. Paris P, Erdogan F (1963) A critical analysis of crack propagation laws. Trans ASME 85(4):528–533
11. Poursaeidi E, Bakhtiari H (2014) Fatigue crack growth simulation in a first stage of compressor blade. Eng Fail Anal 45(1):314–325
12. Irwin GR (1957) Analysis of stresses and strains near end of a crack traversing a plate. J Appl Mech 24:361–364
13. Božić Ž, Schmauder S, Wolf H (2018) The effect of residual stresses on fatigue crack propagation in welded stiffened panels. Eng Fail Anal 84:346–357
14. Zhang XQ, Li L, Qi XL (2017) Experimental and numerical investigation of fatigue crack growth in the cracked gear tooth. Fatigue Fract Eng Mater Struct 40(7):1037–1047
15. Boljanović S, Maksimović S (2014) Mixed mode crack growth simulation with/without overloads. Int J Fatigue 67:183–190
16. Park JH, Atluri SN (1998) Mixed mode fatigue growth of curved cracks emanating from fastener holes in aircraft lap joints. Comput Mech 21(6):477–482
17. Božič Ž, Schmauder S, Mlikota M, Hummel M (2014) Multiscale fatigue crack growth modelling for welded stiffened panels. Fatigue Fract Eng Mater Struct 37(9):1043–1054
18. He XF, Tan MY, Jing TX (2012) An investigation on fatigue crack growth rates through a designed nonsymmetric crack growth test. Eng Fract Mech 96:510–527
19. Boljanović S, Maksimović S (2011) Analysis of crack growth propagation process under mixed-mode loading. Eng Fract Mech 78(8):1565–1576
20. Blažić M, Maksimović S, Petrović Z (2014) Determination of fatigue crack growth trajectory and residual life under mixed mode. Stroj Vestn J Mech Eng 60(4):250–254
21. Zhang XM, Wan L, Yan B (2012) Fracture mechanics. Tsinghua University, Beijing
22. Shantz CRC (2010) Uncertainty quantification in crack growth modeling under multi-axial variable amplitude loading. PhD thesis, Graduate School of Vanderbilt University, Nashville
23. Ayatollahi MR, Razavi SMJ, Yahya MY (2015) Mixed mode fatigue crack initiation and growth in a CT specimen repaired by stop hole technique. Eng Fract Mech 145:115–127
24. NASA (2000) Fatigue crack growth computer program NASGRO version 3.0 reference manual. L.B. Johnson Space Centre, Houston
25. Zhang Z, Liu ZL, Cheng BB (2012) Extended finite element method. Tsinghua University, Beijing
26. Varfolomeev I, Burdack M, Moroz S (2014) Fatigue crack growth rates and paths in two planar specimens under mixed mode loading. Int J Fatigue 58:12–19
27. Budiansky B, Rice JR (1973) Conservation laws and energy-release rates. J Appl Mech 40(1):201–203
28. Zhang X, Li H, Yu XY (2015) Investigation on effect of laser shock processing on fatigue crack initiation and its growth in aluminum alloy plate. Mater Des 65:425–431
29. Zhang XQ, Li H, Duan SW (2015) Modeling of residual stress field induced in Ti–6Al–4V alloy plate by two sided laser shock processing. Surf Coat Technol 280:163–173
30. Mylonas GI, Heckenberger U, Lampeas GN (2010) Investigation on shot-peening induced residual stress field. Int J Microstruct Mater Prop 5(4–5):471–480
31. Zhang X, Chen L, Li S (2015) Investigation of the fatigue life of pre- and post-drilling hole in dog-bone specimen subjected to laser shot peening. Mater Des 88:106–114